GA–A26148

VALIDATING SIMULATIONS OF CORE TOKAMAK TURBULENCE: CURRENT STATUS AND FUTURE DIRECTIONS

by
C. HOLLAND,* J. CANDY, R.E. WALTZ, A.E. WHITE,†
G.R. McKEE,‡ M.W. SHAFER,‡ L. SCHMITZ,†
and G.R. TYNAN*

JUNE 2008

GENERAL ATOMICS

DISCLAIMER

GA–A26148

VALIDATING SIMULATIONS OF CORE TOKAMAK TURBULENCE: CURRENT STATUS AND FUTURE DIRECTIONS

by
C. HOLLAND,* J. CANDY, R.E. WALTZ, A.E. WHITE,†
G.R. McKEE,‡ M.W. SHAFER,‡ L. SCHMITZ,†
and G.R. TYNAN*

This is a preprint of an invited paper presented at the SciDAC 2008, Scientific Computing through Advanced Computing Program in Seattle, Washington, July 13–17, 2008 and to be published in the Proceedings.

*University of California-San Diego, La Jolla, California
†University of California-Los Angeles, Los Angeles, California
‡University of Wisconsin-Madison, Madison, Wisconsin

Work supported by
the U.S. Department of Energy
under DE-FC02-04ER54798, DE-FG02-95ER54309,
DE-FG02-07ER54917, DE-FG03-01ER54615
and DE-FG02-89ER53296

GENERAL ATOMICS PROJECT 30200
JUNE 2008

GENERAL ATOMICS

ABSTRACT

Validating predictive models of turbulent transport in magnetically confined plasmas requires comparisons of detailed fluctuation statistics, in addition to net energy flows. Using measurements from new and improved diagnostics on the DIII-D tokamak [Luxon J L 2002 *Nucl. Fusion* **42** 614], we have performed a series of comparisons against predictions from the GYRO code [Candy J and Waltz R E 2003 *J. Comp. Phys.* **186** 545]. The development and application of synthetic diagnostics that model the spatial sensitivities of a given experimental fluctuation diagnostic is essential for these comparisons. At $r/a = 0.56$, we find very good agreement between the predicted and measured energy fluxes and fluctuation power spectra. However, at $r/a = 0.8$ the simulations underpredict the energy flows by a factor of seven and fluctuation amplitudes by a factor of three, but successfully reproduce the shapes of the experimentally measured fluctuation power spectra. At both locations significant attenuation in the synthetic power spectra and fluctuation levels is observed relative to "unfiltered" levels. Additional results contrasting local and nonlocal simulation results and convergence in toroidal mode number spacing are presented.

1. INTRODUCTION

The development of validated predictive modeling codes has been identified as an essential task for ensuring the success of burning plasma experiments such as ITER [1]. One of the most challenging aspects of this work is the validation of nonlinear simulations of turbulent transport in magnetically confined plasmas. In the absence of large-scale magnetohydrodynamic (MHD) instabilities, the inherent free energy gradients of the confined plasma drive a broad spectrum of nonlinearly interacting small-scale drift-wave instabilities [2] (termed "drift-wave turbulence" hereafter) which in turn drive cross-field flows of particles and energy, limiting the achievable levels of confinement. While these instabilities have received intensive analytic and computational investigation for more than 30 years, it is only in recent years that simulations have matured to the point that they have included what is believed to be the essential physics for making quantitatively accurate predictions of the turbulence and its associated transport. Also essential for validation of these models has been the corresponding maturation of experimental diagnostics able to measure the turbulent fluctuations in relevant parameter ranges, and the advances in computing power to make the "full physics" simulations feasible on tractable timescales.

In order to truly validate a model of drift-wave turbulence, one would like to be able to accurately predict a wide range of fluctuation characteristics, starting with details of the turbulent spectrum such as cross-phases and biphases between different fluctuation fields, to spectral shapes and amplitudes, as well as "higher-order" quantities such as total turbulent flows and fluctuation amplitudes which integrate the lower-order quantities [3]. While there is a long history of comparisons between plasma turbulence measurements and simulation, for large-scale tokamaks these comparisons have been limited by essential physics missing from the simulation (such as equilibrium $\vec{E} \times \vec{B}$ shear), and limited relevant fluctuation measurements. In many cases, the comparisons have been limited to comparisons of predicted energy and particle flows against those determined via a power balance analysis of the measured mean plasma profiles (termed the experimental flows hereafter). Taking advantage of the recent advances in code sophistication, available computing power, and experimental measurements, we have begun taking the next step in turbulence model validation, in which predictions of multiple fluctuation spectra as well as transport levels are compared to experimental measurements. A key aspect for this work is the development of synthetic diagnostics which model the spatial sensitivities of the diagnostics used in these comparisons; including theses sensitivities is essential for meaningful quantitative comparisons.

2. OVERVIEW OF SIMULATION PARAMETERS AND COMPARISONS OF ENERGY FLOWS

The simulations used in this validation exercise were performed with the gyrokinetic turbulence code GYRO [4]. GYRO is a physically comprehensive, nonlinear Eulerian δf initial value code which operates in either a local or nonlocal mode. GYRO was chosen because it is the most physically comprehensive code of its type currently available, able to include all the essential physics necessary for meaningful quantitative comparisons against experiment [5]. This list includes kinetic electrons, realistic electron-ion collisions, electromagnetic effects, equilibrium $\vec{E} \times \vec{B}$ flow shear, the ability to use experimentally measured density, temperature, rotation and E_r profiles as inputs and a realistic magnetic geometry description via the Miller equilibrium model [6]. In this work, we have focused primarily upon local simulations, although we have performed nonlocal ones as well which support the conclusions obtained from the local simulation results. In a local simulation, a $\rho^* = \rho_s / a \rightarrow 0$ limit (where $\rho_s = c_s / \Omega_{ci}$ is the ion gyroradius evaluated at the sound speed $c_s = \sqrt{T_e / M_i}$ and a is the minor radius of the plasma) of the underlying gyrokinetic equations [7] is used to self-consistently eliminate spatial variation in the equilibrium density, temperature, and rotation profiles (with only the local gradient values retained), whereas these variations are retained in the nonlocal simulation. GYRO also allows the user to simulate only a finite subsection of the full torus of the tokamak, using N_n toroidal modes with mode number spacing Δn [i.e., toroidal mode number $n = 0,\ \Delta n,\ 2\Delta n,\ \ldots,\ (N_n - 1)\ \Delta n$]. Choosing a value of $\Delta n > 1$ corresponds to simulating a "wedge" of $2\pi / \Delta n$ extent in toroidal angle, allowing for significant computational savings. We show below that this approximation can be used without impact on the predicted energy flows and net fluctuation amplitudes, consistent with the inherent scale separation between the turbulence and the equilibrium scales.

The experiment modeled is a steady, low-power, sawtooth-free L-mode DIII-D discharge, described in greater detail in Refs. [8] and [9]. A power balance analysis conducted via the ONETWO code [10] is used to determine the rates at which ion and electron energy flow across a given magnetic surface, and are denoted by Q_i and Q_e in this paper. Note that we only reference these net energy flows to avoid any ambiguities in terms of definitions of fluxes or diffusivity coefficients, and to minimize the impact of statistical and systematic errors in the measured plasma profiles and their gradients. Because the power balance calculations rely on an accurate knowledge of the relevant source terms in order to determine these flows, and the source of particles due to edge recycling is not well-constrained, we do not attempt to compare predicted particle fluxes against the power balance results. Although we do not know the particle flux with sufficient accuracy to validate the code predictions, it is expected to be sufficiently small to have a negligible impact on the determination of the energy flows. A comparison of the energy flows predicted by a set of local simulations, as well as an accompanying nonlocal simulation, are shown in figure 1. Each of the local

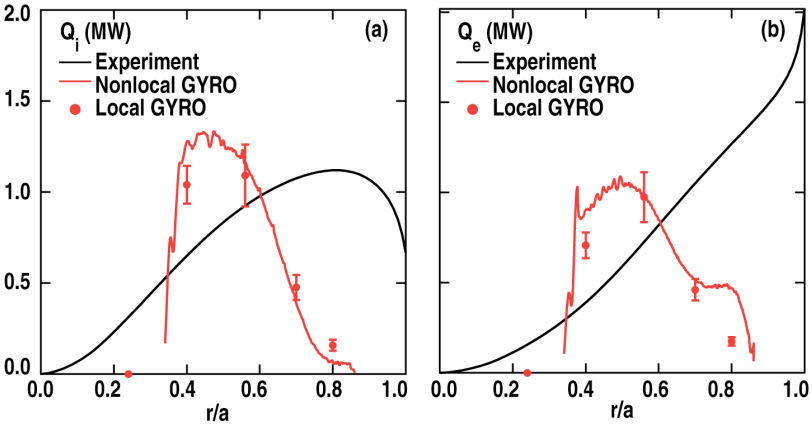

Fig. 1. Comparison of ion (Q_i, a) and electron (Q_e, b) energy flows calculated via ONETWO (black) versus those predicted by GYRO (red).

simulations used 16 toroidal modes, generally spanning a range of $k_y\rho_s$ = [0,1], where $k_y = nq/r$ is the "binormal" wavenumber (i.e., perpendicular to the local magnetic field while still lying in the magnetic flux surface); r is the midplane minor radius and $q = rB_\varphi / rB_\theta$ is the safety factor. All simulations are electromagnetic and use the experimentally measured profiles without modification. The local simulations use a fully realistic mass ratio $\sqrt{M/m} = 60$, while the nonlocal simulation uses $\sqrt{M/m} = 40$ for computational savings. Time integration is done with a fourth order Runge-Kutta algorithm combined with a second order implicit treatment of linear electron physics. The nonlinear terms are discretized using the Arakawa algorithm [11]. A standard 128-point velocity-space discretization is used (8 points in pitch angle, 8 points in energy, and 2 signs of velocity). Further details of the grid resolution and timestep h used, as well as local plasma parameters, can be found in Table 1. The nonlocal simulation uses 24 toroidal modes, spanning a range of $k_y\rho_s$ = [0,1.5] at $r/a = 0.67$. However, because q and ρ_s both vary with r, this resolution is also radially dependant, such that it covers the range $k_y\rho_s$ = [0,3.9] at $r/a = 0.38$ and [0,1.0] at $r/a = 0.85$. We also use a nonuniform radial grid spacing for this simulation such that Δr is proportional to the local value of ρ_s, ranging from $\Delta r/\rho_s(r_0) = 0.88$ at r/a = 0.38 to $\Delta r/\rho_s(r_0) = 0.28$ at $r/a = 0.85$; here $\rho_s(r_0)$ is the gyroradius evaluated at the reference surface $r_0/a = 0.67$.

Table 1. Simulation Parameters

	$r/a = 0.24$	$r/a = 0.4$	$r/a = 0.56$	$r/a = 0.7$	$r/a = 0.8$
expt. Q_i (MW)	0.30	0.65	0.93	1.1	1.1
GYRO Q_i (MW)	0	1.0 ± 0.10	1.1 ± 0.17	0.48 ± 0.068	0.16 ± 0.030
expt. Q_e (MW)	0.15	0.40	0.74	1.0	1.3
GYRO Q_e (MW)	0	0.71 ± 0.071	0.97 ± 0.14	0.46 ± 0.060	0.17 ± 0.023
$\Delta r/\rho_s$	0.54	0.54	0.43	0.48	0.40
L_r/ρ_s	109	108	128	120	121
Δn	2	5	8	10	12
hc_s/a	0.02	0.02	0.02	0.01	0.01

As can be seen from figure 1, there are significant discrepancies between the GYRO predicted and experimental heat fluxes at some locations, with very good agreement occurring at $r/a = 0.56$, but a near factor of 7 under prediction at $r/a = 0.8$. Also of interest is that the nonlocal simulation gives results that are generally consistent in magnitude and variation with radius as the local results. The plotted error bars are the standard deviations of the turbulent fluxes, providing some measure of the variation in time at each location; the nonlocal simulation exhibits a similar level of variability. A local simulation at $r/a = 0.24$ produced no transport, suggesting a complete suppression of the instability by the local $\vec{E} \times \vec{B}$ shear. A significant possible source of some or all of these differences is due to the effects of "profile stiffness," in which a small change in input temperature or density gradient can lead to a much larger change in the observed energy transport [5]. While the statistical errors in the input experimentally measured profile gradients are actually rather small (generally < 5%–6%) [9], larger systematic profile uncertainties remain possible. The one exception to this limitation is the equilibrium $\vec{E} \times \vec{B}$ shear rate, which has a statistical uncertainty on the order of 10%–20%. To better quantify this effect at $r/a = 0.56$, additional runs artificially varying the input $\vec{E} \times \vec{B}$ shear rate and ion temperature scale length $a/L_{Ti} = -a\, d(\ln T_i)/dr$ (the primary driving gradient) were performed. The results of these tests are given in Table 2. While even better agreement at $r/a = 0.56$ can be achieved by changing a/L_{Ti} and $\vec{E} \times \vec{B}$ shear rate within the statistical uncertainties, one in general finds the somewhat surprising result that there is perhaps less stiffness at this location than was observed in previous work. We have also investigated the sensitivity of the $r/a = 0.8$ results, first by reducing the $\vec{E} \times \vec{B}$ shear rate, and then by additionally increasing a/L_{Ti}. The results are shown in Table 3, and while a significant proportional response is observed, the magnitude of the mismatch is such that it is hard to reconcile with small changes to the input gradients, even in the presence of stiff transport.

Table 2. Comparisons of Energy Flows at $r/a = 0.56$

	Experiment (ONETWO)	GYRO (Base)	GYRO (+20% $\gamma_{E\times B}$)	GYRO (+20% $\gamma_{E\times B}$, –5% a/L_{T_i})	GYRO ($\Delta n = 4$)
Q_i (MW)	0.93	1.1 ± 0.17	0.98 ± 0.16	0.79 ± 0.11	1.1 ± 0.13
Q_e (MW)	0.74	0.97 ± 0.14	0.86 ± 0.12	0.75 ± 0.09	1.0 ± 0.10

Table 3. Comparisons of Energy Flows at $r/a = 0.8$

	Experiment (ONETWO)	GYRO (Base)	GYRO (–20% $\gamma_{E\times B}$)	GYRO (–20% $\gamma_{E\times B}$, +10% a/L_{T_i})
Q_i (MW)	1.1	0.16 ± 0.030	0.22 ± 0.031	0.33 ± 0.044
Q_e (MW)	1.3	0.17 ± 0.023	0.23 ± 0.026	0.30 ± 0.031

2.1. Δn CONVERGENCE TEST

Inclusion of all the necessary physics mechanisms significantly increases the computational costs of these simulations relative to earlier simplified studies, with each local run at $r/a = 0.56$ costing approximately 3000 CPU-hours on either the jaguar or franklin CRAY XT4 machines, and the runs at $r/a = 0.8$ costing at least twice as much. While an individual one of these runs may have a small cost relative to so-called "hero" runs, the need to conduct many such runs in order to quantify sensitivities and test convergences quickly accumulates to significant total computational time requirements. Therefore, it is essential to identify avenues to simplify the simulations where possible, without impacting the physics results. One way in which this can be done is to exploit the inherent scale separation of the small-scale drift-wave turbulence and the equilibrium scale lengths, and only simulate a fraction of the full toroidal extent of the plasma. This is done by choosing a toroidal mode number spacing $\Delta n > 1$, and corresponds to simulating a wedge of toroidal extent $\Delta\varphi = 2\pi/\Delta n$. In the local simulations, we have used 16 toroidal modes, with Δn chosen at each location to allow coverage in binormal wavenumber to $k_y\rho_s = 1$. Previous work demonstrated convergence in Δn for a different set of plasma conditions [12]. We have performed an additional test for this particular set of conditions, via a second simulation performed with 32 toroidal modes at $r/a = 0.56$, using $\Delta n = 4$ rather than 8 as was done in the 16-mode case. The ion and electron energy flows plotted as a function of k_y are shown in figure 2 for these two cases, and show an essentially exact match between the two. This can be further quantified by observing that the $\Delta n = 4$ case predicts a $Q_i = 1.1 \pm 0.13$ MW and $Q_e = 1.0 \pm 0.10$ MW, relative to the $\Delta n = 8$ case which predicted $Q_i = 1.1 \pm 0.17$ MW and $Q_e = 0.97 \pm 0.14$ MW (shown in Table 2). Furthermore, we show a similar level of agreement in predicted fluctuation levels and spectra in section 4.

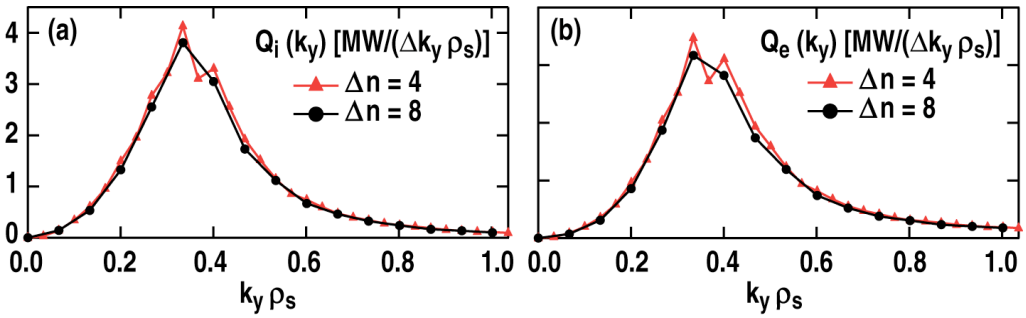

Fig. 2. Comparisons of power spectral densities of Q_i (a) and Q_e (b) at $r/a = 0.56$, calculated using $\Delta n = 4$ (red) and $\Delta n = 8$ (black).

3. GENERATION OF SYNTHETIC DIAGNOSTICS

While the energy flow comparisons presented in section 2 are an important initial step in model validation, comparisons against individual fluctuation field amplitudes and spectra represent a more stringent test of the model. Such comparisons can be made by using data from the beam emission spectroscopy [13] (BES) and correlation electron cyclotron emission [8] (CECE) diagnostics on the DIII-D tokamak [14], which provide spatially localized, high time resolution measurements of density and electron temperature fluctuations, respectively. The BES system consists of a 30 measurement channels arranged in a 5x6 array in the (R,Z) plane with roughly a 1 cm spacing in both directions, while the CECE system consists of a pair of channels radially separated by 0.5 cm. Broadly speaking, each diagnostic measures a specific type of radiation from a small but finite region of the plasma, which can be related to local, instantaneous density or electron temperature fluctuation amplitude. To conduct quantitative comparisons against these measurements, one must use synthetic diagnostics which model what one expects the BES and CECE diagnostics to have measured, if they had observed the turbulence predicted by the simulation. For these specific diagnostics, the synthetic diagnostics consist of transforming the GYRO data from a co-rotating plasma reference frame in which the calculations are performed to the lab reference frame, and accounting for the finite spatial integration volume of each diagnostic channel. The transformation from plasma to lab reference frame is easily done via the formula

$$\delta\hat{X}_l^{LF}(r,\theta,n,t) = \delta\hat{X}_l^{PF}(r,\theta,n,t)e^{-il\Delta n\omega_0 t} \quad , \tag{1}$$

where $\omega_0 = -qcE_r/rB$ is $\vec{E}\times\vec{B}$ rotation rate of the reference surface r_0, $\delta\hat{X}_l^{PF}$ is the complex amplitude of fluctuations with toroidal mode number $n_l = l\Delta n$ in the plasma frame, and $\delta\hat{X}_l^{LF}$ is the corresponding lab-frame amplitude. When applying this transform, it is generally necessary to interpolate the plasma frame data in time, because while the sampling rate of c_s/a at which the GYRO output is saved is more than sufficient to adequately record the time dynamics in the plasma frame without aliasing, it is insufficient for the Doppler-shifted lab-frame rates.

Accounting for the finite integration volumes of each diagnostic is done via the use of "point spread functions" (PSFs), which model the spatial sensitivities of a given diagnostic channel. To create a synthetic signal δX_{syn} corresponding to the diagnostic channel centered at (R_0,Z_0), we first reconstruct the instantaneous real-space representation of the fluctuation field at a specific toroidal angle φ_0 via

$$\delta X_{GYRO}(R,Z,\varphi_0,t) = \sum_{l=-N_n}^{N_n} \delta\hat{X}_l^{LF}(r,\theta,t)e^{-il\Delta n\left[\varphi_0+\nu(r,\theta)\right]} \quad , \tag{2}$$

where $\nu(r,\theta)$ is an eikonal phase function defined by the magnetic geometry model, as is the transformation from (r,θ) coordinate system to the (R,Z) coordinate system. We then convolve δX_{GYRO} with a diagnostic-specific PSF of the form $\psi(R-R_0,Z-Z_0)$, via

$$\delta X_{syn}(R_0,Z_0,\varphi_0,t) = \frac{1}{N_\psi}\iint dRdZ\,\delta X_{\mathrm{GYRO}}(R,Z,\varphi_0,t)\psi(R-R_0,Z-Z_0) \quad , \tag{3}$$

$$N_\psi = \iint dRdZ\,\psi(R-R_0,Z-Z_0) \quad . \tag{4}$$

Further details on how each PSF is calculated can be found in Ref. [9]. This convolution is done for each time t of interest and diagnostic channel to be modeled, generating a set of synthetic timetraces which can then be analyzed in the same fashion as the experimental data. To quantify the effects of the PSFs, the "unfiltered" $\delta X_{\mathrm{GYRO}}(R_0,Z_0,\varphi_0,t)$ values for each diagnostic channel are also recorded. Figure 3 illustrates contours of the PSFs for each diagnostic overlaid on the relevant fluctuation fields. The synthetic diagnostic generation algorithm can be summarized as:

1. Calculate the point spread function $\psi(R-R_0,Z-Z_0)$ for the diagnostic of interest, and the normalization factor N_ψ.
2. Calculate the phase factor $\nu(r,\theta)$.

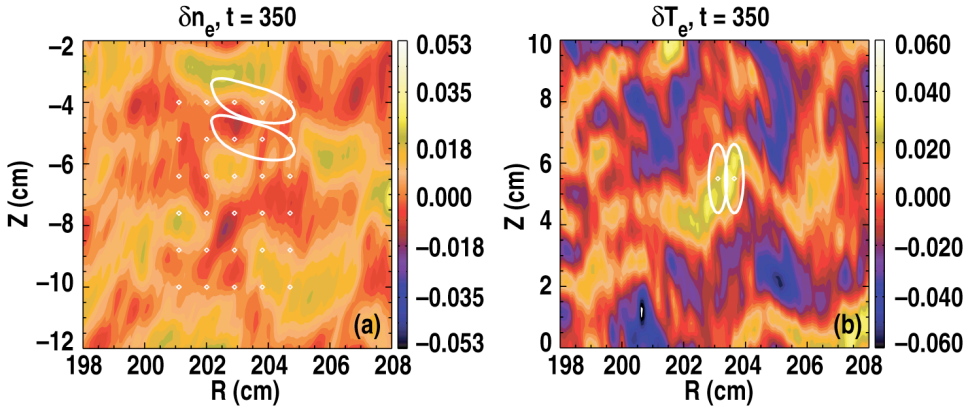

Fig. 3. Contours of electron density fluctuations (a) and electron temperature fluctuations (b) in 10 cm x 10 cm regions of the (R,Z) plane from the local simulation of $r/a = 0.56$. 50% contours of the BES and CECE PSFs are overlaid in white, with diamonds indicating the center locations of the individual diagnostic channels.

For each time t of interest, we then

3. Calculate the lab-frame fluctuation field mode amplitudes $\delta\hat{X}_l^{LF}$, interpolating $\delta\hat{X}_l^{PF}$ in time if necessary.
4. Transform the lab-frame mode amplitudes $\delta\hat{X}_l^{LF}$ into a real-space signal δX_{GYRO} at a specified toroidal angle φ_0 via Eq. (2).
5. Record the unfiltered reference signal $\delta X_{\mathrm{GYRO}}(R_0,Z_0,\varphi_0,t)$.
6. Calculate and record the synthetic signal $\delta X_{\mathrm{syn}}(R_0,Z_0,\varphi_0,t)$ using Eq. (3).

4. COMPARISONS OF LAB-FRAME FLUCTUATION POWER SPECTRA

Comparisons of lab-frame power spectra calculated from the unfiltered GYRO output, synthetic results, and experimental measurements are shown for $r/a = 0.56$ (figure 4). In order to minimize channel-specific noise in the experimental measurements, we compare cross-spectra, defined as $S_{ij}(f) = \left|\langle X_i^*(f) X_j(f)\rangle\right|$ where $X_i(f)$ and $X_j(f)$ correspond to the Fourier transforms of output from two distinct diagnostic channels i and j. In modeling the BES system, we average over all vertically adjacent pairs of channels, while the CECE system uses a pair of radially separated channels. This difference is chosen to minimize the loss of physical signal in the BES measurements, since we expect (and observe) that nearby fluctuations on the same flux surface remain more highly correlated than those on separate ones. To generate additional synthetic data realizations, synthetic time traces are generated at four equally spaced toroidal angles in the simulation, and the results averaged together. As seen in figure 4, we find very good agreement in both the shape and magnitude of the synthetic BES system and the experimental measurements, and somewhat weaker agreement in the CECE system. We also observe a clear attenuation in both spectra due to the averaging effects of the PSFs. This attenuation of power is frequency and diagnostic-dependent, and can be understood in terms of the relative spatial anisotropies of each PSF. The first key to understanding this effect is to note that the significant Doppler shift imposed by the transformation to the lab frame yields a near linear relation $f_{lab} = k_y V_y^{ExB}$, where V_y^{ExB} is the local binormal component of the equilibrium $\vec{E} \times \vec{B}$ velocity. For the BES system, the PSF at $r/a = 0.56$ is predominately elongated radially, and thus its major effect will be to filter out higher radial wave numbers at all k_y (and thus lab-frame frequencies), yielding the relatively uniform attenuation observed. There is a small but finite frequency dependence due to the finite poloidal extent of the PSF as well, but this effect is subdominant to the radial averaging. In contrast, the CECE PSF primarily filters higher k_y, leading to the strong frequency dependence observed for those spectra.

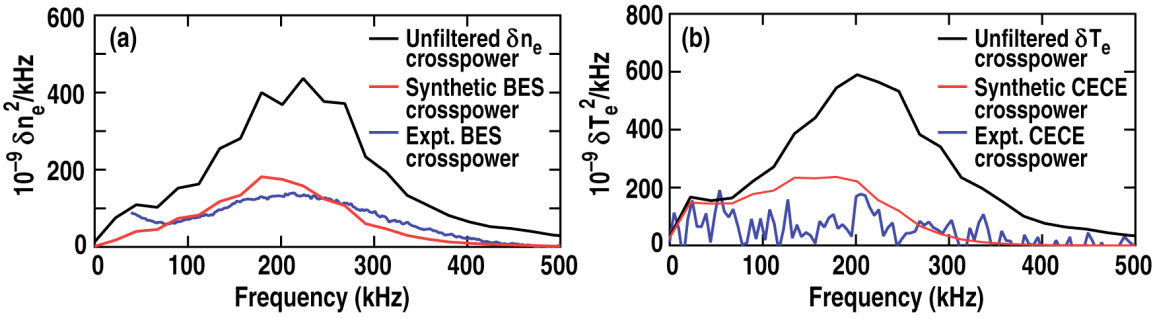

Fig. 4. Comparisons of cross-spectra for density (a) and electron temperature (b) fluctuations for the local $r/a = 0.56$ simulation. The unfiltered GYRO output cross-spectra are shown in black, the synthetic results in red, and experimental measurements in blue.

Because the BES measurements below 40 kHz are significantly impacted by noise in the diagnostic beam, we only compare the spectra between 40 and 400 kHz (where the signal goes below the noise level of the diagnostic); a similar comparison range is used for the CECE system for consistency. To quantify the agreement, we can calculate the root mean square (RMS) fluctuation level associated with fluctuations within that frequency band via formula

$$\delta X^2_{RMS} = \int_{40}^{400} df\, S_{ij}(f) \quad . \tag{5}$$

The results are shown in Table 4. There is a near-perfect level of agreement in the density fluctuation level (0.55% for the synthetic vs. 0.56% for the experiment), whereas the electron temperature fluctuations are over predicted by 40%. However, because the CECE measurement is so close to the noise level, there is a nearly 50% uncertainty in the experimental RMS electron temperature fluctuation level (relative to a 20% uncertainty in the experimental density fluctuation level). It should also be recalled that both the ion and electron energy flows were (slightly) over predicted in this simulation, and that one might expect a better agreement in the electron temperature fluctuation levels if the input profiles had been adjusted to match the experimental energy flows. How strongly this profile adjustment would affect the density fluctuation levels is uncertain. Also note that the unfiltered and synthetic RMS fluctuation levels calculated from the $\Delta n = 4$ simulation are included in Table 5, and are quite close to the $\Delta n = 8$ results. This agreement further highlights the convergence in Δn, and the ability of these wedge simulations to accurately predict integrated quantities like energy flows and fluctuation amplitudes. A comparison of the unfiltered density and electron temperature fluctuation spectra from these cases is shown in figure 5.

Table 4. Comparisons of RMS Fluctuation Levels at $r/a = 0.56$

Level (%)	Unfiltered Cross-Power, 40–400 kHz	Synthetic Cross-Power, 40–400 kHz	Experimental Cross-Power, 40–400 kHz	Unfiltered Cross-Power, $\Delta n = 4$	Synthetic Cross-Power, $\Delta n = 4$
δn	0.90 ± 1.5e-2	0.55 ± 7.7e-3	0.56 ± 0.1	0.98 ± 2.1e-2	0.59 ± 1.1e-2
δT_e	1.1 ± 5.7e-2	0.66 ± 2.4e-2	0.46 ± 0.2	1.1 ± 7.8e-2	0.67 ± 3.2e-2

Table 5. Comparisons of RMS Fluctuation Levels at $r/a = 0.8$

Level (%)	Unfiltered Cross-Power, 30-390 kHz	Synthetic Cross-Power, 30-390 kHz	Experimental Cross-Power, 40-400 kHz
δn	0.69 ± 1.9e-2	0.33 ± 6.9e-3	1.1 ± 0.2
δT_e	0.90 ± 7.7e-2	0.50 ± 1.9e-2	1.6 ± 0.2

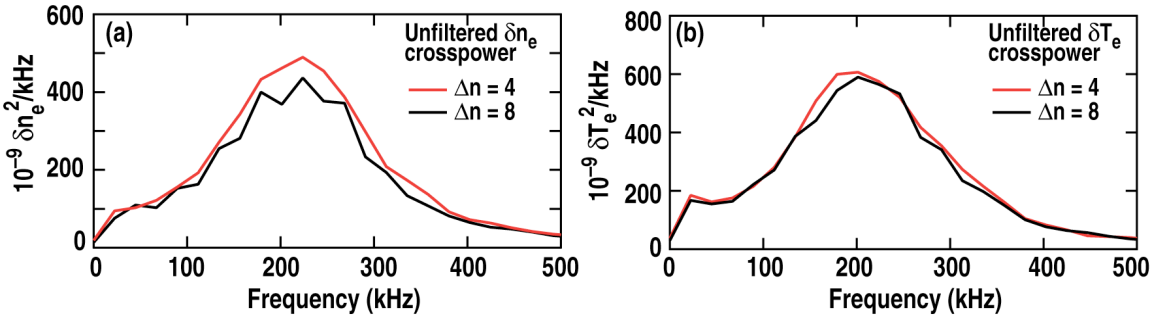

Fig. 5. Comparison of unfiltered cross-spectra of density (a) and electron temperature (b) fluctuations at r/a = 0.56, for $\Delta n = 4$ (red) and $\Delta n = 8$ (black).

A comparison of lab-frame cross-spectra for $r/a = 0.8$ is shown in figure 6. In contrast to the $r/a = 0.56$ results, the fluctuation levels are significantly under predicted; net RMS values are shown in Table 5. Interestingly, the RMS fluctuation levels are under predicted by roughly a factor of three, which is relatively consistent with the factor of seven under prediction in the energy flows. By consistent, we mean that because the turbulent flows are generally observed to scale with fluctuation amplitude squared, a factor of seven under prediction in the flows should lead to a generic under prediction of fluctuation levels by $\sqrt{7} = 2.64$, close to the observed factor of 3. Even more interestingly, if we rescale the synthetic fluctuation spectra to contain the same amount of power as the experimental spectra (shown as the purple curves in figure 6), we find very good agreement between the shapes of the synthetic and experimental spectra. Keeping in mind the strong correlation between lab-frame frequency and poloidal mode number, we also observe a very good agreement between poloidal correlation functions calculated with the synthetic and experimental data (Ref. [9]). A stronger frequency dependence observed in the attenuation of the synthetic BES signal can be understood in terms of the PSF at this location exhibiting a more symmetric shape than at $r/a = 0.56$. Current work is focused on understanding why the simulations under predict the fluctuation levels and energy flows at $r/a = 0.8$ so significantly. Some possibilities are discussed in greater detail in Ref. [9], including potentially missing long-wavelength modes such as resistive ballooning modes or insufficient range in simulated k_y, neither of which we deem likely due to $\vec{E} \times \vec{B}$ shear suppression and an inability to increase ion energy transport, respectively. Other candidates include systematic errors in the power balance calculations, the use of an overly simplified electron collision operator in the GYRO simulations, and nonlocal effects coupling the turbulence dynamics at $r/a = 0.8$ to the strong variations in equilibrium profiles and normalized turbulent intensity at larger radii. We also hope to conduct even finer tests of simulation predictions in the near future, by comparing against experimental measurements of fluctuation cross phases that are crucial components in setting the levels of turbulent flows.

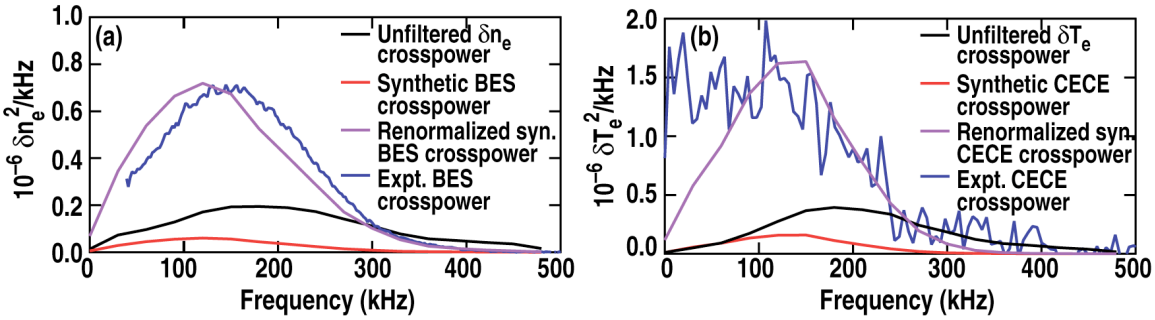

Fig, 6. Comparisons of cross-spectra for density (a) and electron temperature (b) fluctuations for the local $r/a = 0.8$ simulation. The unfiltered GYRO output cross-spectra are shown in black, the synthetic results in red, and experimental measurements in blue. The synthetic spectra rescaled to contain the same power in the 40-400 kHz band as the experimental results are shown in purple.

5. CONCLUSIONS

Advances in computational models of turbulent plasma transport, coupled with recent increases in available computing power and new and improved fluctuation diagnostics, opens the door to the next level of model validation, simultaneous quantitative comparisons of turbulent fluxes and individual fluctuation field characteristics. The development and application of synthetic diagnostics that model the experimental ones are essential for accurate, meaningful quantitative comparisons between code and experiment. Using newly developed synthetic BES and CECE diagnostics, we have shown that a "full physics" GYRO simulation which accurately predicts the total energy flows Q_i and Q_e at $r/a = 0.56$ also successfully reproduces measured fluctuation characteristics, including fluctuation level and spectral shapes. In a second case in which the energy flows were significantly under predicted at $r/a = 0.8$, the RMS fluctuation amplitudes were likewise under predicted in a "self-consistent" manner, but the shapes of the fluctuation power spectra were still rather accurately predicted. Understanding the physics underlying the differing levels of success of these simulations in reproducing the experimental observations, and conducting additional validation studies for a broader range of plasma conditions are the next steps for this research, and will be presented in future publications.

REFERENCES

[1] Shimada M *et al*. 2007 *Nucl. Fusion* **47** S1

[2] Horton W 1999 *Rev. Mod. Phys*. **71** 735

[3] Terry P W *et al*. 2008 *Phys. Plasmas* **15** 062503

[4] Candy J and Waltz R E 2003 *J. Comp. Phys*. **186** 545

[5] Candy J and Waltz R E 2003 *Phys. Rev. Lett*. **91** 045001

[6] Miller R L, Chu M S, Greene J M, Lin-Liu Y R, and Waltz R E 1998 *Phys. Plasmas* **5** 973

[7] Brizard A J and Hahm T S 2007 *Rev. Mod. Phys*. **79** 421

[8] White A E *et al*. 2008 *Phys. Plasmas* **15** 056116

[9] Holland C *et al*. 2008 Implementation and application of two synthetic diagnostics for validating simulations of core tokamak turbulence, submitted to *Phys. Plasmas*

[10] St John H E, Taylor T S, Lin-Liu Y R, Turnbull A D 1994 *Plasma Phys. Controlled Nucl. Fusion Res*. **3** 603

[11] Arakawa A 1966 *J. Comput. Phys*. **1** 119

[12] Waltz R E, Austin M E, Burrell K H, and Candy J 2006 *Phys. Plasmas* **13** 052301

[13] McKee G R *et al*. 2007 *Plasma Fusion Res*. **2** S1025

[14] Luxon J L 2002 *Nucl. Fusion* **42** 614

ACKNOWLEDGMENTS

This work supported by the U.S. Department of Energy under DE-FC02-04ER54798, DE-FG02-95ER54309, DE-FG02-07ER54917, DE-FG03-01ER54615 and DE-FG02-89ER53296. The authors would like to thank T.L. Rhodes, W.A. Peebles, E.J. Doyle, R. Prater, J.C. DeBoo, K.H. Burrell, P.H. Diamond, J.E. Kinsey, G.M. Staebler, D.R. Mikkelsen, R.V. Bravenec, and R.V. Budny for many useful discussions. A.E. White's research was performed under appointment to the Fusion Energy Sciences Fellowship Program administered by Oak Ridge Institute for Science and education under a contract between the U.S. Department of Energy and the Oak Ridge Associated Universities. This research used resources of the National Center for Computational Sciences at Oak Ridge National Laboratory, which is supported by the Office of Science of the Department of Energy under Contract DE-AC05-00OR22725, and the National Energy Research Scientific Computing Center, which is supported by the Office of Science of the U.S. Department of Energy under Contract No. DE-AC02-05CH11231.